Journal of Materials Chemistry A

Accepted Manuscript

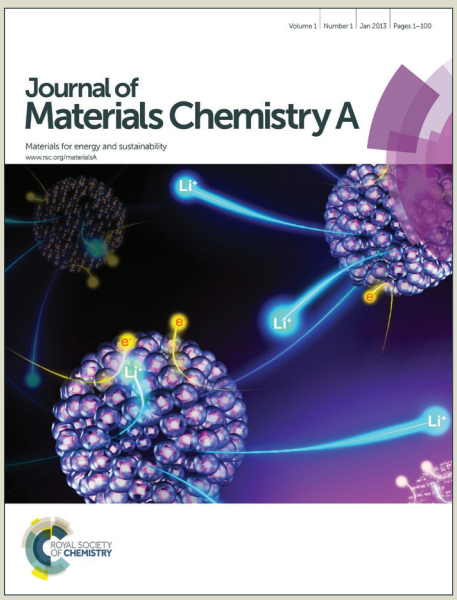

ROYAL SOCIETY OF CHEMISTRY

www.rsc.org/materialsA

Journal Name

ARTICLE

Mesoporous NiO single-crystalline utilized as noble metal-free catalyst for non-aqueous Li-O_2 battery†

Received 00th January 20xx,
Accepted 00th January 20xx

DOI: 10.1039/x0xx00000x

www.rsc.org/

Shengfu Tong,[a,‡] Mingbo Zheng,[b,‡] Yong Lu,[a] Zixia Lin,[b] Jun Li,[b] Xueping Zhang,[a] Yi Shi,[b] Ping He[a,*] and Haoshen Zhou[a,c]

Mesoporous NiO nanosheet with single-crystalline structure was investigated as oxygen electrode catalyst in non-aqueous Li-O_2 battery. The recharge voltage plateau achieved on the NiO-based Li-O_2 battery was ca. 3.95 V, ca. 200 mV negatively shifted compared with that on the β-$Ni(OH)_2$ and acetylene black. The reaction mechanism during charge process for NiO-based Li-O_2 battery was intensively researched. The results of X-ray photoelectron spectroscopy characterization indicated that Li_2O_2 and Li_2CO_3 were formed during the discharge process, which can be decomposed after recharge. These demonstrated that the NiO nanosheet exhibited a good activity for decomposition of Li_2O_2 and Li_2CO_3. Furthermore, the results of gas chromatography-mass spectrometer test reflected two steps of recharge process, i.e., the oxidation of Li_2O_2 when the potential was below 4.0 V and the decompositions of Li_2O_2 and Li_2CO_3 when the potential was above 4.0 V. Moreover, no obvious performances decay was observed on the NiO-based battery even after 40 cycles when the capacity was limited by 500 mAh·g^{-1}, indicating an impressive cycling performance.

Introduction

Rechargeable non-aqueous lithium-oxygen (Li-O_2) batteries, the theoretical gravimetric energy reaches ca. 3,600 Wh·kg^{-1} based on the reversible reaction (equation 1),[1, 2] is increasingly very attractive in recent years owing to the potential applications in electric-vehicle, which can decrease the dependence on fossil fuel for human beings.[3-8] Typical non-aqueous Li-O_2 battery consists of Li metal anode, lithium salt contained non-aqueous electrolyte, catalysts loaded cathode, and current collector. A freshly assembled Li-O_2 battery is under a charged status that can output energy directly. During the discharge process, O_2 is reduced (known as oxygen reduction reaction, ORR) after entering the system and combines with Li^+ in the electrolyte to form insoluble Li_2O_2 at cathode which can be decomposed during charge process.[3] The main reactions occurred at the electrodes during discharge are given as equation (2) and (3). Despite the efforts have been dedicated during the past decade, challenges such as low round-trip efficiency, low rate capability, poor cycle life, and electrolyte instability etc., still existed in the system,[5, 9] which should be solved before Li-O_2 batteries can be extensively applied.

$$2Li + O_2 \rightarrow Li_2O_2 \quad (1)$$

Anode: $Li \rightarrow Li^+ + e^-$ (2)

Cathode: $O_2 + 2Li^+ + 2e^- \rightarrow Li_2O_2$ (3)

The overpotential energy loss of ORR and oxygen evolution reaction (OER), taken place at the cathode on discharge and charge processes, are serious issues in Li-O_2 batteries.[10-18] Decreasing the overpotential of ORR and OER with effective catalysts is critical to enhance the discharge and recharge performances of Li-O_2 batteries. It was reported that noble metals and metal oxide (e.g., α -Mn_2O_3) exhibited activity to ORR,[10, 11, 19] and especially noble metals can suppress the formation of Li_2CO_3 without carbon in the electrode,[11] which is very important to improve the cycle life of the system. It is necessary to emphasize that these catalysts for ORR also exhibit activity to OER,[10, 13, 20-23] and it is considered that the electrical efficiency of the system can be promoted by reducing the overpotential of OER.[24] Therefore, more efforts have been focused on recharge process, and the catalysts commonly studied are carbon,[25, 26] titanium-based materials,[14, 27] and soluble redox mediators,[28-33] as well as the noble metals and transition metal oxides mentioned above. It is generally considered that noble metal-based materials, e.g., Au, Ru and RuO_2, exhibited superior activity for OER and can improve the properties of the system.[1, 13, 20] Obviously, high cost of these noble metal based catalyst limits their practical application. Thus, developing highly effective and low cost catalysts for promoting OER was necessary and eagerly demanded.

Transition metal oxide, e.g., MnO_2, Co_3O_4 and NiO etc., caused attentions owning to their advantages such as low-cost, easy availability, environmental benign nature and cost effectiveness. Particularly, MnO_2 and Co_3O_4 exhibits catalytical activity in Li-O_2 batteries as reported recently.[23, 34, 35] However, the recharge plateau is still at a relatively positive potential, or lack of activity/evidence for the decomposition of Li_2CO_3.[36, 37] In contrast,

[a] National Laboratory of Solid State Microstructures, College of Engineering and Applied Sciences, Collaborative Innovation Center of Advanced Microstructures, Nanjing 210093, China. *E-mail: pinghe@nju.edu.cn
[b] School of Electronic Science and Engineering, Nanjing University, Nanjing 210093, China.
[c] Energy Technology Research Institute, National Institute of Advanced Industrial Science and Technology (AIST), Umezono 1-1-1, Tsukuba 305-8568, Japan.

†Electronic Supplementary Information (ESI) available: The SEM and TEM images of NiO, and the recycle discharge-recharge curves capacity limited by 200 mAh·g^{-1} are included. See DOI: 10.1039/x0xx00000x

‡ These authors contributed equally to this work.

NiO was considered to be active for the decomposition of Li_2CO_3, but rare reports concerned it in Li-O_2 batteries.[24, 38]

In this paper, oxygen electrode was composed of a noble metal free catalyst with porous structural nanosheets nickel oxide, which was synthesized by a facile alcohol-thermal method, and the performances of mesoporous structural NiO in non-aqueous Li-O_2 battery were investigated in detail. The NiO exhibited the catalytic activity to decompose Li_2O_2 and Li_2CO_3, and the recharged plateaus was more negative than 4.0 V vs. Li/Li^+. Furthermore, the performances of the system kept almost identical after 40 continuous discharge-recharge cycles when the capacity was limited by 500 mAh·g^{-1}. The results achieved in this study revealed the potential applications of porous structural NiO in Li-O_2 batteries.

Experimental

Porous NiO sheets were synthesized from $Ni(NO_3)_2{\cdot}6H_2O$ and NaOH (AR, Nanjing Chemical Reagent Co., Ltd., P.R. China) by means of facile alcohol-thermal method with ethanol as the dispersant. $Ni(NO_3)_2{\cdot}6H_2O$ and NaOH were mixed in mol ratio of 1:2, and kept at 180°C for 24 hr to obtain the intermediate β-$Ni(OH)_2$, followed by heating at 300°C for 1 hr with temperature increasing rate of 1°C·min^{-1} after pre-dried at 60°C.[39] The as-prepared NiO sheets were used as the main component for oxygen electrode. The oxygen electrode material was consisted of 70 wt.% NiO, 20 wt.% acetylene black (AB, Alfa Aesar) and 10 wt.% polytetrafluoroethene (PTFE emulsion, 12%) binder, and the capacity of the Li-O_2 battery was normalized by carbon. CR2032-type coin cells with holes for oxygen transfer, assembled in a glove box filled with dry Ar, were used to evaluate the electrochemical performances. Before assembling, the electrode material got dried at 80°C overnight. Stainless steel supplied by Shenzhen Kejing Star Corp (Wisdom opto-electronic technology Ltd.) and polypropylene was used as current collectors and separator, respectively. Tetraethyleneglycol dimethyl ether (TEGDME) (from Aldrich) mixed with $LiCF_3SO_3$ in mol ratio of 4 : 1 was used as electrolyte. LAND 2001A Battery Testing Systems (Wuhan LAND electronics Co., Ltd, P.R. China) were utilized for electrochemical performances tests.

The structure, morphology, and specific surface area were characterized by X-ray diffraction (XRD) (D8 Advance, Bruker), transmission electron microscope (TEM) (JEM-200CX , JEOL), scanning electron microscope (SEM) (SU8010, Hitachi) and N_2 adsorption/desorption Brunauer-Emmett-Teller (BET) (ASAP 2020HD88, Micromeritics). The state of surface elements were characterized by X-ray photoelectron spectroscopy (XPS) spectra which were recorded using a Thermo Fisherscientific Model K-Alpha spectrometer equipped with Al Kα radiation (1486.6 eV). The in-situ gas chromatography-mass spectrometer (GC-MS) measurements were carried out with a homemade cell connected to the equipment from PerkinElmer (Clarus 680 and SQ 8S). The O_2 supplied for discharge was ultrapure O_2 (>99.995%, Jiangsu Institute of Metrology, Nanjing, P. R. China), and the concentration of H_2O was controlled to be lower than 0.1 ppm. All the electrochemical measurements were carried out under room temperature.

Results and discussion

Characterizations of NiO nanosheets

Figure 1a displays the XRD patterns of the intermediate β-$Ni(OH)_2$ (red) and NiO (black) obtained by alcohol-thermal method. The XRD patterns of both β-$Ni(OH)_2$ and NiO are similar as previous study,[40] and index to the cubic phased NiO. Figure 1b exhibited the N_2 adsorption/desorption curves of β-$Ni(OH)_2$ and NiO, the specific surface area of NiO based on BET results was ca. 188 m^2 g^{-1} which was almost 4 times larger than that of β-$Ni(OH)_2$ (ca. 40 $m^2{\cdot}g^{-1}$). The higher specific surface area of NiO than that of β-$Ni(OH)_2$ can be due to the porous structure formed during the heating treatment, which was further confirmed by TEM characterizations, and will be further discussed.

Figure 2a shows the TEM image of typical NiO nanosheets which had a hexagonal shape. The SEM and TEM images of as-prepared NiO nanosheets were also available in Fig. S1. From the TEM images, it can be seen that the nanosheets exhibit an average width of ca. 200 nm, and the angle of adjacent edge is approximate 120 degree. The magnified image of an individual nanosheet in Fig. 2b reveals that the nanosheet has a mesoporous structure. The selected-area electron-diffraction (SAED) techniques detected at several positions on the nanosheets show the same diffraction pattern as shown in Fig. 2c, corresponding to the [111] zone axis of monocrystal particle. The geometry of the nanosheets is consistent with previous studies,[40, 41] in which the porous structure was attributed to the formation of Ni-O-Ni cross-linkage bridges during the thermal process on the $Ni(OH)_2$. Thus, the nanosheets were grown along the (111)-plane, which corresponded to the close packing direction but not the Ni-O-Ni bond directions. Such porous structure is expected to provide sufficient channels for oxygen transition, which has positive effect on Li-O_2 batteries.

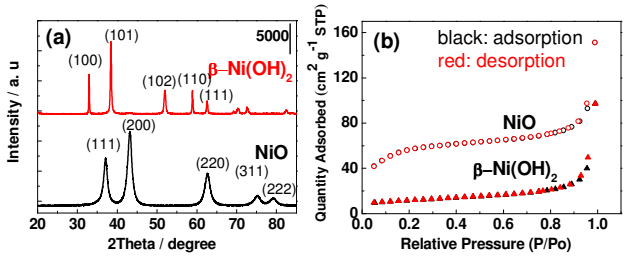

Fig. 1 The (a) XRD patterns and (b) BET curves of intermediate β-$Ni(OH)_2$, (triangle) and as-prepared NiO (circle), respectively.

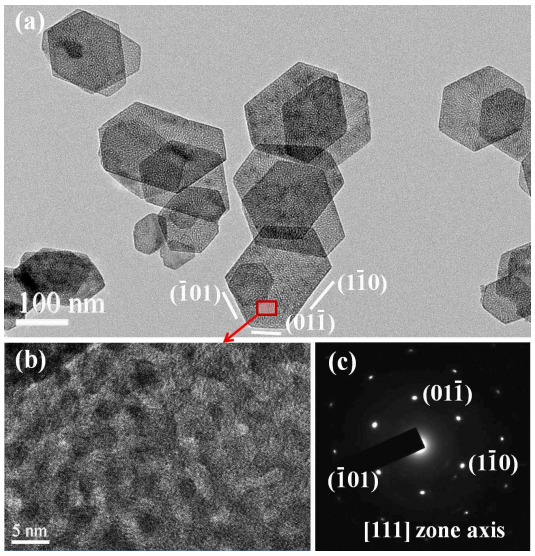

Fig. 2(a) TEM image of the NiO nanosheets, where most of nanosheets exhibit a hexagonal shape. (b) The enlarged view of an individual nanosheets. The nanosheet is observed as a mesoporous structure (c) The corresponding SAED pattern along the [111] axis direction.

Electrochemical performances of NiO in Li-O_2 batteries

Figure 3a depicts the first cycles of potential cut-off galvanostatic discharge-recharge voltage curves on AB (black curve), β-$Ni(OH)_2$/AB (blue curve) and NiO/AB (red curve) based Li-O_2 batteries at a current of 100 mA·g^{-1}. It can be seen that the discharge plateau on NiO/AB was identical as that on AB (2.65 V), while that on β-$Ni(OH)_2$/AB was 2.55 V. As for the recharge process, the plateaus on NiO/AB was ca. 3.95 V, negatively shifted by ca. 200 mV compared with that observed on AB and β-$Ni(OH)_2$/AB, even comparable with that achieved on carbonized bacterial cellulose supported Ru nanoparticles based Li-O_2 battery.[2] This revealed that NiO played as catalytical role in the recharge process of Li-O_2 battery, while β-$Ni(OH)_2$ showed relatively lower or even without activity to OER. On the other hand, the specific capacity on NiO/AB (ca.1260 mAh·g^{-1}) was 1.6 and 6.7 times larger than that observed on AB (ca. 480 mAh·g^{-1}) and β-$Ni(OH)_2$/AB (ca. 165 mAh·g^{-1}), which may be due to the large surface area of NiO compared with that of AB (76.8 m^2 g^{-1}) and β-$Ni(OH)_2$. Figure 3b is the SEM image of NiO/AB based oxygen electrode after discharge process, as the D-point in Fig. 3a. The products (e.g., Li_2O_2) were not clearly observed from the SEM image, however, the hexagonal structure of nanosheets NiO was remained, which can also be obviously recognized even after recharge process (see Fig. S2), implying the good mechanical stability of NiO nanosheets in the system.

To confirm the products obtained from the NiO/AB based Li-O_2 battery and investigate the mechanism of OER on NiO, XPS spectra of Li1s, C1s, O1s, and Ni2p were recorded, and the corresponding results were illustrated in Fig. 4. The black line- scatters were the raw XPS spectra for the samples obtained at D- (a, c, e, and g) and R- (b, d, f and h) point in Fig. 3a, and the solid curves were the simulation and the best fitting results. The peaks at 54.8 and 55.6

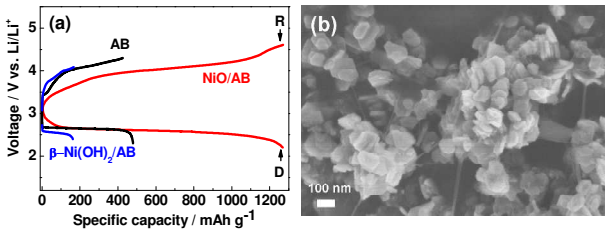

Fig. 3(a) First cycles of potential cut-off galvanostatic discharge-recharge voltage curves with AB (black curve), β-$Ni(OH)_2$/AB (blue curve) and NiO/AB (red curve) as O_2 electrode at current of 100 mA·g^{-1}. (b) SEM image of NiO/AB based oxygen electrode after discharge.

eV in Fig. 4a can be assigned to Li1S of the products Li_2O_2 and Li_2CO_3 (due to the oxidation of AB component in the electrode), respectively,[42, 43] which confirmed to the results shown in Fig. 4c and 4e. In Fig. 4c, the peak at 284.4 eV can be assigned to AB, that at 286.1 and 292.4 eV can be attributed to the electrolyte, while the peak at 289.8 eV was due to the product of Li_2CO_3.[44] In Fig. 4e, the peaks at 529.3 and 531.3 eV can be assigned to the O in NiO-based

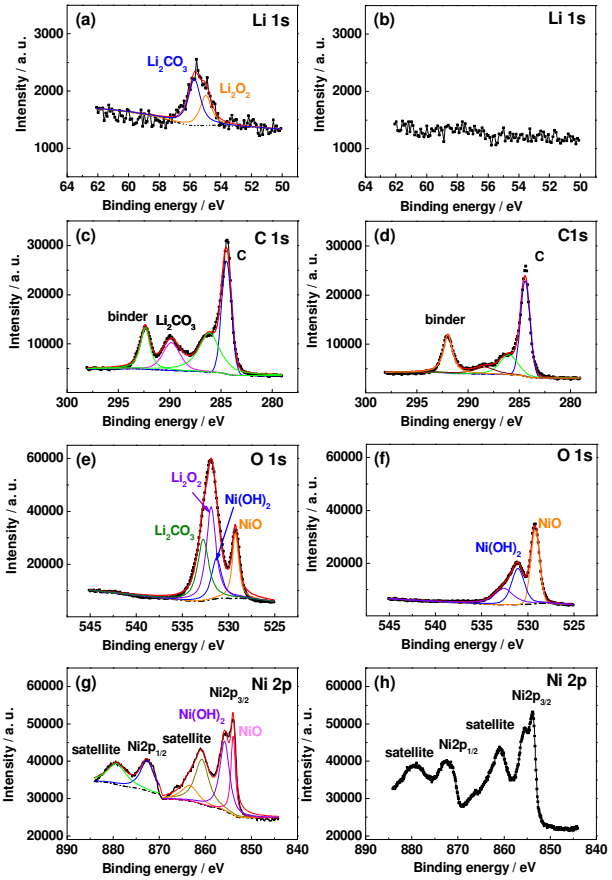

Fig. 4(a) XPS spectra of Li 1s (a and b), C 1s (c and d), O 1s (e and f) and Ni 2p (g and h). Figure 4a, c, e, and g are the results of the sample after discharge process (D-point in Fig. 3a), while figure 4b, d. f and h are the results of the sample after recharge process (R-point in Fig. 3a). The dot curves are the raw data, the dash dot curve is the background, and the red solid curves are the fitting results.

material (i.e., NiO and $Ni(OH)_2$),[45] and the peaks at 531.7 and 532.7 eV can be attributed to the products of Li_2O_2 and Li_2CO_3, respectively.[43] Fig. 4g illustrated the Ni2p XPS spectra, the Ni $2p_{3/2}$ main peak and its satellite at 853.8 eV and 861 eV, and the Ni $2p_{1/2}$ main peak and its satellite at 872.8 and 879.5 eV, are in agreement to the previously reported values,[44, 45] which can be attributed to the Ni in its oxide.[44] The peaks at 855.6 and 879.6 eV in Fig. 4d can be assigned to the signal of nickel in $Ni(OH)_2$, respectively.[44-47] These results observed on Li1s, C1s and O1s indicated that the discharge products on NiO/AB consist of Li_2O_2 and Li_2CO_3, and the products were suggested to deposit on the disk plate of NiO, rather than in the porous.

It is obvious that in Fig. 4b, d, f, and h, the peaks due to the products of Li_2O_2 and Li_2CO_3 were disappeared after recharge process, while the others remained. This reflected a good catalytic performance of NiO/AB for the decomposition of Li_2O_2 and Li_2CO_3. Take a look at Fig. 4g and 4h, it is surprise to find that the Ni2p XPS spectra for the discharged and recharged products were similar, indicating analogical components in these two samples. It is curious to find the catalytical part in the as-prepared NiO. The discrepancy of electrochemical performance of Ni(II) between β-$Ni(OH)_2$ and NiO (Fig. 3a), suggesting the vital role in OER on NiO-based electrode should not be β-$Ni(OH)_2$. The detail mechanism of OER on NiO-based material need to be further studied.

The catalytic properties of NiO on decomposition of Li_2O_2 and Li_2CO_3 were also supported by in-situ GC-MS measurements, and the corresponding results were exhibited in Fig. 5. The recharge process can be divided into part I and part II. When the potential was more negative than 4.0 V (part I), the gas with mass weight of 32 (O_2) was detected without observation of 44 (CO_2), indicating the oxidation of Li_2O_2. When the potential was more positive than 4.0 V

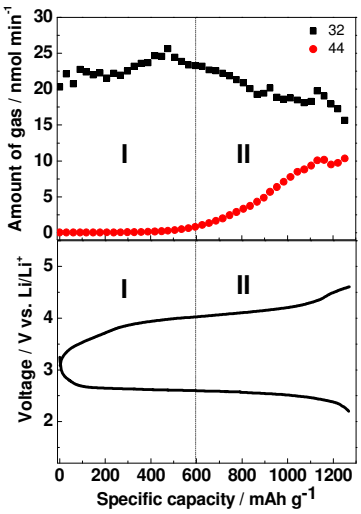

Fig. 5 The in-situ GC-MS results for the NiO/AB based Li-O_2 battery. The bottom panel is the potential cut-off galvanostatic discharge-recharge voltage curves with NiO/AB as O_2 electrode at current of 100 mA·g^{-1}. The top panel is the relative amount of the species with mass 32 (black) and 44 (red) as a function of specific capacity, which were recorded simultaneously during charge process.

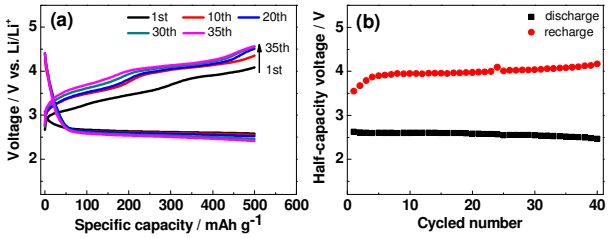

Fig. 6(a) The continuously cycled discharge-charge curves with cut-off capacity of 500 mAh·g^{-1} of the non-aqueous Li-O_2 battery with NiO as the oxygen cathodic material, the current applied for discharge and charge was 100 mA·g^{-1}; (b) the relation between the half-capacity voltage and the cycled times during the continuously cycled discharge-recharge performances.

(part II), the amount of O_2 started declining and that of CO_2 got increasing, reflecting the decomposition of Li_2O_2 and Li_2CO_3 were involved during recharge process. The results discussed above demonstrated that NiO exhibited a good catalysis for the decomposition of Li_2O_2 and Li_2CO_3 during charge process, in good agreement with very recent work reported,[24] and implying NiO can be a good candidate for non-aqueous Li-O_2 battery. The decomposition of Li_2CO_3 may be expressed by equation (4), as proposed in previous study,[48] though the detailed mechanism need to be further investigated.

$$2Li_2CO_3 \rightarrow 4Li^+ + 2CO_2 + O_2 + 4e^- \quad (4)$$

The relationship between the amount of O_2 generated and that of charge passed during recharge process can be estimated from Fig. 5, and the corresponding result is shown in Fig. S3. The fitting line gave a slope of ca. 0.36, which was smaller than that of theoretical value for oxidation of Li_2O_2, i.e., 0.50. This suggested that subsidiary reaction probably occurred during recharge process, which may result in the decay of the system during cyclic performances.

Figure 6a shows the continuously cycled discharge-recharge curves of the non-aqueous Li-air battery with NiO/AB as the oxygen cathodic material at current of 100 mA·g^{-1}, the specific capacity of the cell was controlled at 500 mAh·g^{-1}. It is clear that the NiO based Li-O_2 battery kept a stable performance even after 35 cycles. The cycled number dependent half-capacity voltage shown in Fig. 5b also reflected unconspicuous polarization during continuously performances. If the specific capacity was limited by 200 mAh·g^{-1}, the performances can be retained till the 100 cycles (Fig. S4). These results indicated a good life time cycling of NiO oxygen electrode, which showed a good agreement with the results discussed in Fig. 4. The good stability and low cost, as well as the high activity for decomposition of Li_2O_2 and Li_2CO_3 during charge process, implied the potential applications of NiO in non-aqueous Li-O_2 batteries.

Conclusions

Summarily, mesoporous NiO nanosheets with single-crystalline were synthesized by a facile alcohol-thermal method. The specific surface area of as-prepared NiO was 188 m^2 g^{-1} which was almost 4 times larger than that of precursor β-$Ni(OH)_2$ (40 m^2·g^{-1}). The mesoporous NiO nanosheets as cathodic catalyst of Li-O_2 battery delivered a reversible capacity of 1260 mAh·g^{-1} and a charge voltage

plateau of 3.95 V. The performances of NiO based battery kept almost identical after 40 discharge-recharge cycles when the capacity was limited by 500 $mAh \cdot g^{-1}$. The reaction mechanism during charge process for NiO-based Li-O_2 battery can be illuminated with ex- and in-situ methods. The XPS dates indicated that Li_2O_2 and Li_2CO_3 were formed during the discharge process, which can be decomposed after recharge. The results of GCMS test reflected two steps of recharge process, i.e., the oxidation of Li_2O_2 when the potential was below 4.0 V and the decompositions of Li_2O_2 and Li_2CO_3 when the potential was above 4.0 V. All the researches suggested that the mesoporous NiO nanosheets with single-crystalline exhibited potential applications as noble metal-free catalyst for non-aqueous Li-O_2 battery.

Acknowledgements

This research was partially supported financially by Chinese National Key Fundamental Research Project (2014CB932302 and 2014CB932303), National Natural Science Foundation of China (21373111, 21403106, 21403107 and 51202106), Natural Science Foundation of Jiangsu Province of China (BK2012309 and BK20140055), and the Fundamental Research Funds for the Central Universities (20620140622 and 20620140625).

Notes and references

1 Z. L. Jian, P. Liu, F. J. Li, P. He, X. W. Guo, M. W. Chen and H. S. Zhou, *Angew. Chem. Int. Edit.*, 2014, **53**, 442-446.
2 S. F. Tong, M. B. Zheng, Y. Lu, Z. X. Lin, X. P. Zhang, P. He and H. S. Zhou, *Chem. Commun.*, 2015, **51**, 7302-7304.
3 K. M. Abraham and Z. Jiang, *J. Electrochem. Soc.*, 1996, **143**, 1-5.
4 Y. G. Wang, Y. Y. Xia, *Nat. Chem.* 2013, **6**, 445-447.
5 J. Lu, L. Li, J. B. Park, Y. K. Sun, F. Wu and K. Amine, *Chem. Rev.*, 2014, **114**, 5611-5640.
6 J. J. Wang, Y. L. Li, X. L. Sun, *Nano Energy*, 2013, **4**, 443-467.
7 M. Armand and J. M. Tarascon, *Nature*, 2008, 451, 652-657.
8 P. G. Bruce, S. A. Freunberger, L. J. Hardwick and J. M. Tarascon, *Nat. Mater.*, 2012, **11**, 19-29.
9 P. G. Bruce, L. J. Hardwick and K. M. Abraham, *Mrs Bull.*, 2011, **36**, 506-512.
10 Y. C. Lu, H. A. Gasteiger and Y. Shao-Horn, *J. Am. Chem. Soc.*, 2011, **133**, 19048-19051.
11 J. Xie, X. H. Yao, I. P. Madden, D. E. Jiang, L. Y. Chou, C. K. Tsung and D. W. Wang, *J. Am. Chem. Soc.*, 2014, **136**, 8903-8906.
12 N. A. Galiote, D. C. de Azevedo, O. N. Oliveira and F. Huguenin, *J. Phys. Chem. C*, 2014, **118**, 21995-22002.
13 Z. Q. Peng, S. A. Freunberger, Y. H. Chen and P. G. Bruce, *Science*, 2012, **337**, 563-566.
14 M. M. O. Thotiyl, S. A. Freunberger, Z. Q. Peng, Y. H. Chen, Z. Liu and P. G. Bruce, *Nat. Mater.*, 2013, **12**, 1049-1055.
15 F. J. Li, T. Zhang and H. S. Zhou, *Energ. Environ. Sci.*, 2013, **6**, 1125-1141.
16 B. D. McCloskey, D. S. Bethune, R. M. Shelby, G. Girishkumar and A. C. Luntz, *J. Phys. Chem. Lett.*, 2011, **2**, 1161-1166.
17 B. D. McCloskey, D. S. Bethune, R. M. Shelby, T. Mori, R. Scheffler, A. Speidel, M. Sherwood and A. C. Luntz, *J. Phys. Chem. Lett.*, 2012, **3**, 3043-3047.
18 T. Zhang and H. S. Zhou, *Nat. Commun.*, 2013, **4**, 1817.
19 M. Augustin, O. Yezerska, D. Fenske, I. Bardenhagen, A. Westphal, M. Knipper, T. Plaggenborg, J. Kolny-Olesiak and J. Parisi, *Electrochim. Acta*, 2015, **158**, 383-389.
20 F. J. Li, D. M. Tang, Y. Chen, D. Golberg, H. Kitaura, T. Zhang, A. Yamada and H. S. Zhou, *Nano Lett.*, 2013, **13**, 4702-4707.
21 Y. C. Lu, Z. C. Xu, H. A. Gasteiger, S. Chen, K. Hamad-Schifferli and Y. Shao-Horn, *J. Am. Chem. Soc.*, 2010, **132**, 12170-12171.
22 F. Jiao and P. G. Bruce, *Adv. Mater.*, 2007, **19**, 657-660.
23 A. Debart, A. J. Paterson, J. Bao and P. G. Bruce, *Angew. Chem. Int. Edit.*, 2008, **47**, 4521-4524.
24 M. Hong, H. C. Choi and H. R. Byon, *Chem. Mater.*, 2015, **27**, 2234-2241.
25 J. B. Park, J. Lee, C. S. Yoon and Y. K. Sun, *Acs Appl. Mater. Inter.*, 2013, **5**, 13426-13431.
26 R. R. Mitchell, B. M. Gallant, C. V. Thompson and Y. Shao-Horn, *Energ. Environ. Sci.*, 2011, **4**, 2952-2958.
27 F. J. Li, R. Ohnishi, Y. Yamada, J. Kubota, K. Domen, A. Yamada and H. S. Zhou, *Chem. Commun.*, 2013, **49**, 1175-1177.
28 Y. H. Chen, S. A. Freunberger, Z. Q. Peng, O. Fontaine and P. G. Bruce, *Nat. Chem.*, 2013, **5**, 489-494.
29 D. Sun, Y. Shen, W. Zhang, L. Yu, Z. Q. Yi, W. Yin, D. Wang, Y. H. Huang, J. Wang, D. L. Wang and J. B. Goodenough, *J. Am. Chem. Soc.*, 2014, **136**, 8941-8946.
30 H. D. Lim, H. Song, J. Kim, H. Gwon, Y. Bae, K. Y. Park, J. Hong, H. Kim, T. Kim, Y. H. Kim, X. Lepro, R. Ovalle-Robles, R. H. Baughman and K. Kang, *Angew. Chem. Int. Edit.*, 2014, **53**, 3926-3931.
31 M. J. Lacey, J. T. Frith and J. R. Owen, *ElectroChem. Commun.*, 2013, **26**, 74-76.
32 M. Z. Yu, X. D. Ren, L. Ma and Y. Y. Wu, *Nat. Commun.*, 2014, **5**, 5111.
33 N. N. Feng, P. He and H. S. Zhou, *Chemsuschem*, 2015, **8**, 600-602.
34 H. W. Park, D. U. Lee, L. F. Nazar and Z. W. Chen, *J. Electrochem. Soc.*, 2013, **160**, A344-A350.
35 T. Maiyalagan, K. A. Jarvis, S. Therese, P. J. Ferreira and A. Manthiram, *Nat. Commun.*, 2014, **5**, 3949.
36 A. Debart, J. Bao, G. Armstrong and P. G. Bruce, *J. Power Sources*, 2007, **174**, 1177-1182.
37 C. Q. Shang, S. M. Dong, P. Hu, J. Guan, D. D. Xiao, X. Chen, L. X. Zhang, L. Gu, G. L. Cui and L. Q. Chen, *Sci. Rep.*, 2015, **5**, 8335.
38 D. F. Qiu, G. Bu, B. Zhao, Z. X. Lin, L. Pu, L. J. Pan and Y. Shi, *Mater. Lett.*, 2015, **141**, 43-46.
39 M. B. Zheng, Ph. D Thesis, Nanjing University of Aeronautics and Astronautics, 2009.
40 N. D. Hoa and S. A. El-Safty, *Chem. Eur. J.*, 2011, **17**, 12896-12901.
41 D. W. Su, M. Ford and G. X. Wang, *Sci. Rep.-Uk*, 2012, **2**, 924.
42 R. Younesi, S. Urbonaite, K. Edstrom and M. Hahlin, *J. Phys. Chem. C*, 2012, **116**, 20673-20680.
43 K. P. C. Yao, D. G. Kwabi, R. A. Quinlan, A. N. Mansour, A. Grimaud, Y. L. Lee, Y. C. Lu and Y. Shao-Horn, *J. Electrochem. Soc.*, 2013, **160**, A824-A831.
44 J. F. Moyulder, W. F. Stickle, P. E. Sobol and K. D. Bomben. Handbook of X-ray Photoelectron Spectroscopy, J. Chastain, Ed.: Physical Electronics: ULVAC-PHI, Chigasaki. 1995.
45 M. A. Peck and M. A. Langell, *Chem. Mater.*, 2012, **24**, 4483-4490.
46 X. Sun, G. K. Wang, J. Y. Hwang and J. Lian, *J. Mater. Chem.*, 2011, **21**, 16581-16588.
47 L. Zhang, K. Xiong, S. G. Chen, L. Li, Z. H. Deng and Z. D. Wei, *J. Power Sources*, 2015, **274**, 114-120.
48 S. Meini, N. Tsiouvaras, K. U. Schwenke, M. Piana, H. Beyer, L. Lange and H. A. Gasteiger, *Phys. Chem. Chem. Phys.*, 2013, **15**, 11478-11493.

TOC:

Porous-structured NiO nanosheets, synthesized by means of a facile alcohol-thermal method, was utilized as noble metal free catalyst for non-aqueous Li-O_2 battery. The NiO showed good activity to Li_2O_2 and Li_2CO_3.